ADVANCED FUNCTIONAL MATERIALS
www.afm-journal.de

www.MaterialsViews.com

# The Importance of Bridging Points for Charge Transport in Webs of Conjugated Polymer Nanofibers

*Jean-Christophe Bolsée, Wibren D. Oosterbaan, Laurence Lutsen, Dirk Vanderzande, and Jean Manca**

**Electrical characterizations on webs of highly ordered semiconducting polymer nanofibers (NFs) are often performed with large electrodes devices (millimeter scale) for which the carrier transport is an average between transport within isolated NFs and transport at the intersection of two or more NFs. In order to assess the nanoscale electrical properties of the NFs, a field-effect transistor based on conductive atomic force microscopy is introduced that allows the visualization of the current distribution at the nanometer scale within a web of poly(3-butylthiophene) NFs. The contact resistance is evaluated to be ≈4 kΩ cm, which does not limit the charge transport process, and the mobility in one single NF is $\mu_{NF} = 0.07 \pm 0.03$ cm$^2$ V$^{-1}$ s$^{-1}$. One NF can carry a current density of 20 kA cm$^{-2}$ without being destroyed. Moreover, by observing the current maps in detail, it is found that the electrical resistance associated with the bridging of two or more individual NFs does not reduce the charge transport inside the web of NFs. Finally, different kinds of bridging geometries are shown and the role of tie molecules is discussed.**

## 1. Introduction

Recently, much attention has been directed towards the synthesis and characterization of one-dimensional (1D) nanostructures fabricated from conjugated polymers and small organic molecules. Their unique properties, such as high aspect ratios and chemical and mechanical stability, make them candidates for high performance components for future organic devices such as solar cells,[1,2] photodetectors,[3] and transistors.[4]

A typical example of these 1D nanostructures are the nanofibers (NFs) of regioregular poly(3-alkylthiophene)s (RR-P3*A*Ts), which crystallize in solution.[5–8] Processing NFs from fiber dispersions offers good control of the film morphology. P3*A*Ts denote a class of conjugated polymers where the number of carbon atoms in the alkyl side chain can vary. By far, the most famous representative is poly(3-hexylthiophene) (P3HT) with six carbon atoms, followed by poly(3-butylthiophene) (P3BT) with four carbon atoms on the alkyl side chain. The crystal structure of a P3BT NF is sketched in **Figure 1**. They consist of folded or extended polymer chains stacked along the fiber length by $\pi$–$\pi$ interaction and two to three layers of the polymer stacks separated by the butyl side chain along the alkyl stacking direction.[9]

In addition to their future applications, these highly ordered NFs offer an ideal tool for investigating charge transport phenomena in field-effect transistor structures.[9,10] Webs of P3*A*T NFs have been intensively studied and mobility values in the range 0.04 ± 0.02 cm$^2$ V$^{-1}$ s$^{-1}$ were reported by different groups.[6,10,11] However, the employed organic field-effect transistors (OFET) devices have much larger dimensions (channel width $W$ (mm) and channel length $L \approx 10$ μm) than the dimensions of a typical NF (width 20 nm, length (μm)).[8] Consequently, charge transport in an OFET device involves transport through two processes: within individual NFs and interfiber transport at the intersection of two or more NFs. The impact of these bridging points on the effective transport is unknown and subject to discussion.[10,12,13]

In order to address these questions, we introduce a transistor where one of the electrodes is the mobile conductive atomic force microscopy (CAFM) tip. It enables one to resolve the current distribution at the nanometer scale within a web of P3BT NFs and to evaluate the role of bridging points in charge transport within a web of NFs. The CAFM-transistor is applied on polymer NFs but we consider that this can be used on every electrically active nanostructures for which electrical characterizations at the nanoscale are needed.

## 2. Results and Discussion

CAFM is a current sensing AFM technique where a metal-coated tip scans the sample and measures simultaneously sample conductivity and topography under a certain voltage.[14,15] CAFM can be used in two modes: the first mode, called imaging mode, consists in applying a constant voltage to the sample while the tip is scanning. The topography and current images are simultaneously recorded and allow correlating the highly conducting regions with the topographical features. In the second mode,

J.-C. Bolsée, Dr. W. D. Oosterbaan, Prof. D. Vanderzande
Prof. J. V. Manca
Hasselt University
Campus Diepenbeek
Institute for Materials Research
Agoralaan Building D, 3590 Diepenbeek, Belgium
E-mail: jean.manca@uhasselt.be
Dr. L. Lutsen, Prof. D. Vanderzande, Prof. J. V. Manca
IMEC-IMOMEC
Wetenschapspark 1, 3590 Diepenbeek, Belgium

DOI: 10.1002/adfm.201102078

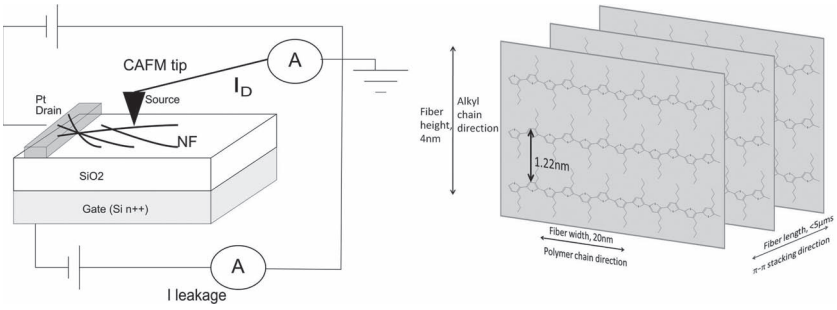


**Figure 1.** Schematic of the CAFM field-effect transistor with one electrode being the mobile CAFM tip. Schematic of a P3BT nanofiber.[9]

called spectroscopic mode, the tip is fixed at one point and the sample voltage is swept across a certain range giving an current/voltage ($I/V$) characteristic.

In a first step, a qualitative description of our CAFM field-effect transistor is given of samples obtained from a high concentration dispersion (0.005 wt%). Its capability to resolve the current distribution at the nm scale and the appearance of the transistor effect (increase of NFs conductivity by a negative $V_G$) will be demonstrated. In a second step, we focus on samples obtained from a lower concentration dispersion (0.001 wt%) and measure the contact resistance $R_C$ and NF in-plane mobility, $\mu_{NF}$. Finally, in a third step, we evaluate the role of bridging points between NFs on charge transport.

### 2.1. Transistor with CAFM Tip Electrode: Proof of Concept

To study charge transport along the NFs, a transistor structure like the one depicted in Figure 1 is used. It consists of a highly n-doped Si gate electrode with a $SiO_2$ gate dielectric (gate capacitance per unit area $C_o = 16.9\,nF\,cm^{-2}$). A self-assembled monolayer of hexamethyldisilazane (HMDS) is used to passivate $SiO_2$. Using conventional photolithography, a thin drain electrode (10 nm Pt layer on top of a 2 nm Ti adhesion layer) is patterned. The electrode is made as thin as possible to improve electrode connection and to avoid the disruption of the NFs since their thickness is close to 4 nm. Compared to a standard FET device with two fixed electrodes, our set-up has one mobile electrode, which is the CAFM tip. While scanning across the sample, the current flowing from the CAFM tip to the Pt drain electrode via the NFs is measured. Two voltage sources and associated current meters were used: one was internal to the atomic force microscope and one was external (Keithley 2400 sourcemeter). Both power supplies were grounded on the tip potential. To determine the transistor transfer characteristics for which the gate voltage, $V_G$, was swept at a fixed drain voltage, $V_D$, the AFM source was connected to $V_G$ and the external one to $V_D$. While to determine the output characteristics for which $V_D$ was swept at different fixed $V_G$, both power supplies were switched.

The NFs are randomly drop-cast on the substrate. Due to their high surface coverage, they form a 2D web connected to the drain electrode even at a distance of hundreds of micrometers from the electrode. **Figure 2** shows three typical CAFM measurements in the imaging mode. In the first zone, the correlation between the topography image (panel A) and the current image (panel B) is excellent: the current is zero when the tip is not touching any NFs and becomes positive as soon as a NF is reached. Some NFs, such as the ones circled in panel A, are not connected to the drain electrode and consequently the associated current in B is zero. The correlation is also outstanding for zone 2 (compare panels C and D) and zone 3 (compare panels E and F). In other words, it is possible to measure the current distribution with nanometer resolution and in particular through isolated NFs.

A second key point shown in Figure 2 is the conductivity enhancement of the NFs when the $V_G$ is decreased as this is expected for p-type semiconductors. On D, $V_G$ is progressively decreased from 0 V to –12 V leading to a current increase by a factor 10 while on F the NFs are alternately switched from insulating to conducting by changing the gate voltage between 0 V and –10 V.

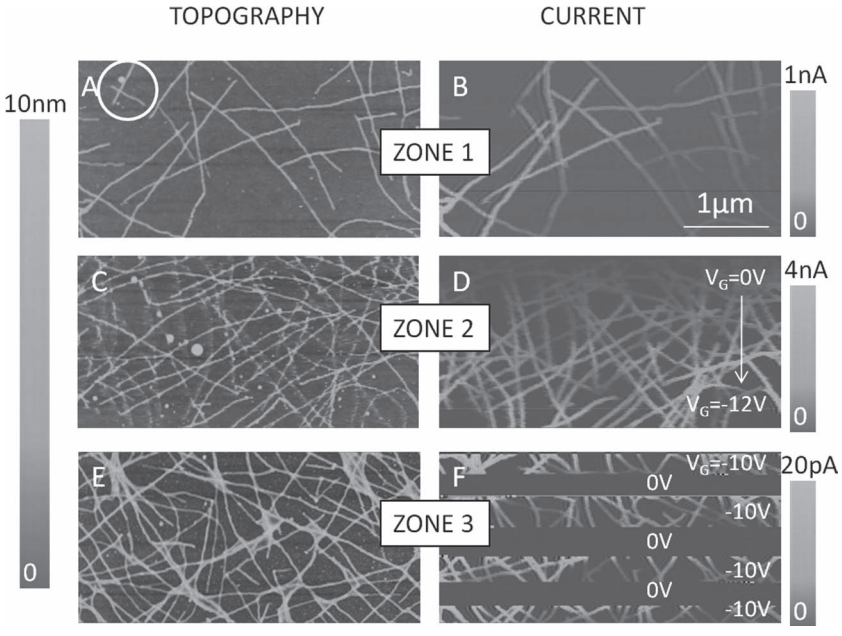


**Figure 2.** Topography and corresponding current images obtained on P3BT NFs on $SiO_2$ at various $V_D$ and $V_G$ conditions. A,B) Zone 1: $V_D = 2$ V and $V_G = -4$ V are fixed. C,D) Zone 2: the fibers conductivity is increased as $V_G$ is decreased progressively from top to bottom with $V_D$ fixed at 4 V. E,F) Zone 3: as $V_G$ is changed from –10 V to 0 V, the NFs are switched from on to off states with $V_D$ fixed at 4 V.

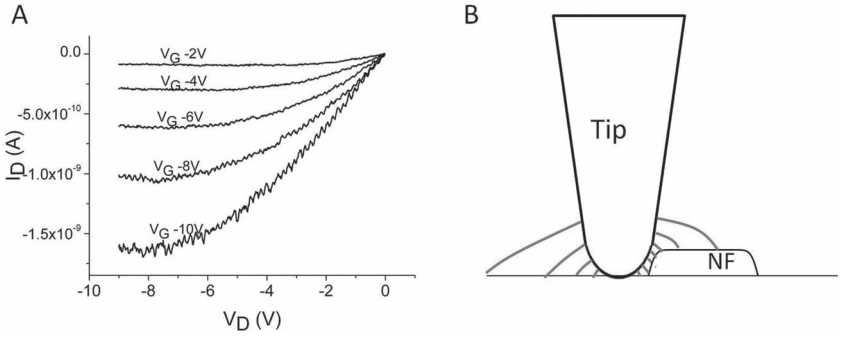


**Figure 3.** A) Output characteristic for a fixed CAFM tip position on a P3BT NF showing the expected linear and saturation behaviors for a p-type semiconductor working in accumulation mode. B) Field lines in the vicinity of the CAFM tip.

An important question for current transport through nanofibers is to know whether the measurements are destructive or not for the NFs. To address this point, we image two times the same area at fixed $V_D$ and $V_G$ and compare the two current maps. By changing $V_D$ and $V_G$, the mean value of the current map can be tuned. It is found that for mean current up to 4 nA, the second map keeps the same signature as the first one but with a slight current reduction. This hysteresis is a well-known phenomenon in organic transistors where hole trapping causes the transistor current to continuously decrease under constant bias conditions.[16] Therefore, the observed current reduction is not attributed to NFs destruction. On the other hand, for current approaching 5 nA, a current drop to 0 A is inevitably observed. Consequently, the maximum current is 4 nA, which leads to current density $J_{max} = \frac{I_{max}}{Wh} = 20$ kA cm$^{-2}$ with $W = 20$ nm one fiber width and $h = 1$ nm the thickness of the accumulation layer. This is widely accepted and reported that in OFETs conduction mainly occurs in the first nanometer of the semiconducting layer from the dielectric interface.[17,18] The reasons are that both the charge carrier density and field-effect mobility are significantly reduced at 1 nm depth perpendicular from the interface compared to interface values.[17] Since the conductivity is proportional to the product of the mobility and the carrier concentration, it explains that conduction occurs in the first nanometer. This result is valid for undoped semiconductors placed in field-effect devices operating in the linear regime and does not depend on the lateral dimensions of the investigated structure and, thus, is also applicable for the nanofibers.

All the measurements shown in Figure 2 are for positive drain voltage where the holes are emitted from the drain electrode and collected at the tip. There is no hole injection barrier from the Pt drain electrode (work function ≈5.6 eV) into the polymer highest occupied molecular orbital (HOMO) level (≈5.2 eV). For negative drain voltage, less stable and reproducible results were obtained probably because of the high work function of the drain electrode, which hampers hole collection, or due to a high contact resistance at the tip NFs junction, which limits holes injection. Therefore, most of the data presented here are made with positive drain voltage. We are aware that the denominations "drain" and "source" electrodes as sketched in Figure 1 could be controversial because for positive $V_D$ holes are emitted from the side electrode and collected at the tip electrode. However, this nomenclature is kept because our source electrode is grounded as this is usually the case.

In the spectroscopic mode, an output characteristic can be performed at a fixed tip position (**Figure 3**A). In order to deplete the channel at the drain side and thus visualize the saturation regime, it is necessary to sweep $V_D$ within negative values. The obtained curves are those of a p-type semiconductor with current amplification for negative $V_G$, which confirms once again that a transistor with one mobile electrode has been constructed.

It is observed in almost all the current maps that the "electric width" (defined as the width of one NF measured in the current map) is larger than the "geometric width" (as measured in the topography map), which is also larger than the true NF width due to tip broadening.[19] The typical deviation between electric and geometric width is 6–8 nm (3–4 nm on each side). It corresponds to a situation where current is detected while the CAFM tip is still pressing on the substrate, as is sketched in Figure 3B. A tunneling current is expected to occur for a tip–NF distance less than 1 nm. This is one contribution to the difference between geometric and electric width. The second occurs when the tip touches one NF and indents it along a certain lateral distance until the force exerted on the tip is high enough to be detected. At this moment, the AFM controller lifts the tip and the geometric width is detected.

### 2.2. Estimation of the Contact Resistance ($R_C$)

Due to the limited contact size at the tip contact (contact radius ≈2 nm, see Experimental Section) and the short length of the NFs, the question of contact resistance effect is relevant.[20,23] Before trying to extract any mobility values from our data, we have to prove that the measurements are not contact limited. The total resistance $R_{tot}$ is the sum of the contact resistance $R_C$ and the channel resistance: $R_{tot} = R_C + R_{channel} = R_C + \frac{\rho L}{Wh}$ where $L$ is the channel length (length of the NF in this section), $W$ is the channel width (width of the NF), and $\rho$ is the resistivity of the NFs. Since a current map displays the current in the NFs as a function of the length of the NFs, it is possible to estimate $R_C$ as the value of $R_{tot}$ at zero length. **Figure 4** explains the strategy to determine the contact resistance $R_C$. First, topography and current maps are taken close to the drain electrode (panels A and B) but without reaching it to avoid instabilities. Then, the drain electrode is partially imaged to measure the channel length (panel C). Finally, we zoom in on the NFs to be studied (panels D and E). Panels F and G show the current profile along top and bottom NFs where the extrapolation to zero length gives $R_C \approx 1$ GΩ ± 1 GΩ. Considering the worst case $R_C \approx 2$ GΩ, this gives $R_C W \approx 4$ kΩ cm, which is of the same order of magnitude as the reported values for standard organic transistors.[21] Although $R_C$ seems huge, the worst case value is only 5% of $R_{tot}$ when we measure 100 pA at $V_D = 4$ V, which is typical for CAFM measurements. It is worth noting that the same behavior was observed on many different samples.

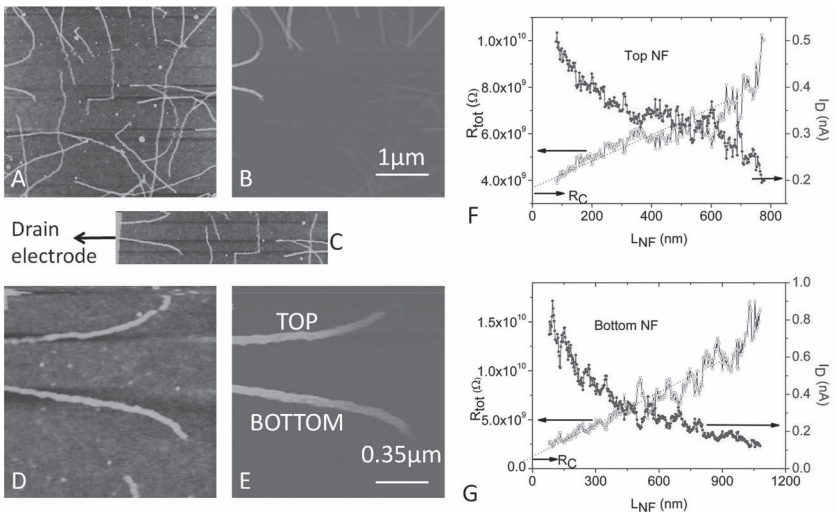


**Figure 4.** Estimation of contact resistance from current images at fixed bias for P3BT NFs on $SiO_2$. A) Topography and B) corresponding current images for $V_G = -4$ V and $V_D = 2$ V. The drain electrode is out of the image on the left. C) Topography image of a part of A with the drain electrode on the left extremity. No bias is applied when imaging the drain electrode to avoid instabilities. D) Zoomed topography and E) corresponding current images of (C) showing two NFs. The drain electrode is 80 nm on the left of the image. F,G) Current profiles along both individual NFs where it is clear that the current increases as the tip approaches the drain electrode. $L_{NF}$ denotes the length of the NF starting from the drain electrode. From the extrapolation of $R_{tot}$ to $L_{NF} = 0$, we obtain $R_C \approx 1\ G\Omega \pm 1\ G\Omega$.

zero as expected for an ideal transistor. Based on this good matching, we can conclude that our NFs do not suffer from oxygen and water contamination (as expected from our home-made glove box), which are known to move $V_T$ towards positive $V_G$, and that the NFs are hole and electron traps free since hole and electron traps would move $V_T$ toward negative and positive $V_G$, respectively.[16]

Finally, the mobility is obtained by fitting $\mu_{NF} = \frac{L}{WC_o V_D} \cdot \frac{\partial I_D}{\partial V_G}$ from the slope of the transfer characteristic. The measurement was repeated on about ten different isolated NFs and led to a mean value of $\mu_{NF} = 0.07 \pm 0.03\ cm^2\ V^{-1}\ s^{-1}$.

CAFM was already applied to P3HT mesowires synthesized by template wetting.[23] The authors found a mobility $\approx 2 \times 10^{-5}\ cm^2\ V^{-1}\ s^{-1}$ and a contact resistance ≈10 GΩ, which is high enough to limit the transport. Although applied on the same class of polymers, these results are in contradiction with our data. The discrepancy is explained by the absence of gate electrode in the set-up of ref. [23], which changes all the transport processes (lower $\mu$ and higher contact resistance) since the carrier concentration is much smaller.[24]

Therefore, we can conclude that the measurements are not contact limited.

### 2.3. Hole Mobility in one Single NF ($\mu_{NF}$)

One of the main goals of our mobile electrode transistor is to measure the longitudinal mobility in one isolated NF ($\mu_{NF}$). **Figure 5** shows the followed strategy. In a first step, the target NF has to be imaged up to the electrode. This is done in panel A without voltage bias to avoid any instabilities which would be caused by the metal-metal contact. Then, once the target NF is identified the tip is positioned at the desired location and $V_G$ is swept to give the transfer characteristic in panel B. $V_D$ is chosen small enough such that the transistor operates in the linear regime. Before extracting $\mu_{NF}$, two important points can be discussed. It can be seen in panel B that the transfer characteristic does not suffer from contact resistance effects. If it was the case, then the absolute slope on the linear scale $\left|\frac{\partial I_D}{\partial V_G}\right|$ would decrease at high negative $V_G$, which is not the case in Figure 5. Another transistor parameter commonly reported is the threshold voltage $V_T$, defined as the intersection of the transfer characteristic with zero current. From Figure 5, we obtain a value of –2 V ± 1 V which has to be corrected to –4 V ± 1 V.[22] These results are close to

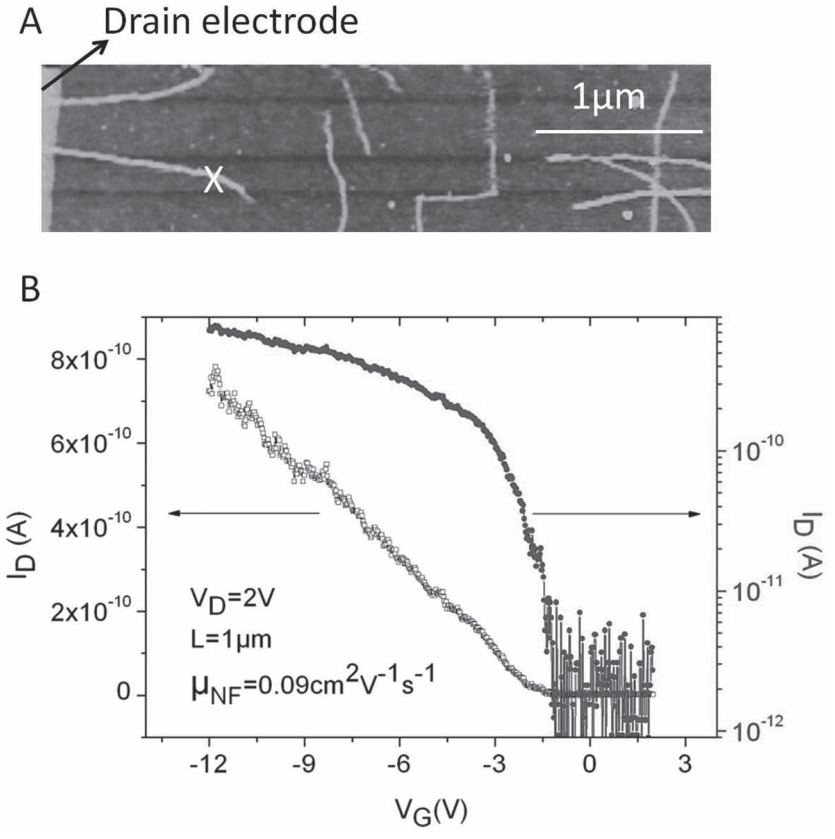


**Figure 5.** Mobility measurement on one single P3BT NF. A) Topography map showing one isolated NF connected to the drain electrode at the left extremity. B) Transfer characteristic from which the mobility is fitted on the point labeled X in (A).

### 2.4. Influence of Bridging Points on Charge Transport

The main benefit of the CAFM based transistor is that one can visualize the current distribution at the nm scale and, as will be demonstrated, it allows us to evaluate the electrical resistance of bridging points of NFs.

For each pixel of a current map a current $I(x,y)$ is obtained, which can be converted into an equivalent electrical resistance using the relation

$$R_{eq}(x, y) = V_D / I(x, y) \quad (1)$$

An important question is to know what influences $R_{eq}(x,y)$. When flowing from the tip, fixed on point P, to the drain electrode, the current is split at each bridging point (defined as the intersection of two or more NFs) and follows different percolation pathways until the drain electrode is reached. The electrically active web between the tip and the drain electrode is composed of $n$ bridging points each having a resistance $R_{bp}$ and $m$ NF segments of length $l$ with a length-dependent intrinsic resistance $R_{NF}(l)$. $R_{eq}$ at point P is influenced by all these elements:

$$R_{eq,p} = f(n, R_{bp}, m, R_{NF}(l), R_C) \quad (2)$$

The electrical resistance of a bridging point, $R_{bp}$, can be estimated by comparing the CAFM currents at the different sides of a bridging point.

If the tip–electrode distance is large (more than 10 µm) and the NFs concentration is high (as in Figure 2), then $n$ and $m$ can be as high as $10^4$ and $10^5$. These numbers are so large that even if the transport was limited by bridging points, no current variation would be detected. On the other hand, measurements taken at low concentration and close to the drain electrode bring quantitative information. In **Figure 6** the currents at the four poles (points 1, 2, 3, and 4) of a typical bridging point are compared: $I_1 = 430$ pA, $I_2 = 420$ pA, $I_3 = 430$ pA, and $I_4 = 395$ pA. The four equivalent resistances of the four poles are deduced by looking at the topographical image. For instance, when the tip is on point 1, $R_{eq,1}$ is the parallel association of four different pathways (the ones going through 2, 3, 4, and the one to the drain electrode). It is clear that the resistance of the short pathway to the drain electrode is much smaller than the three others pathways hence $R_{eq,1} = R_{NF}(300\text{ nm})$ with 300 nm the length between point 1 and the drain electrode, as deduced from the topography map. A similar reasoning holds for point 2, 3, and 4 for which the bridging point contribution has to be added: $R_{eq,2} = R_{eq,3} = R_{eq,4} = R_{NF}(300\text{ nm}) + R_{bp}$. Using Equation (1) for the four poles, it is possible to calculate $R_{NF}(300\text{ nm}) = 4.6$ GΩ and $R_{bp} = 0.4$ GΩ. In other words, the electrical resistance of the bridging point is much smaller than the one of a segment of NF.

To gain more confidence in this result, the analysis has been repeated many times on other samples, **Figure 7** and **Table 1**. The mathematical expressions for $R_{eq,i}$ have been obtained from the careful reading of the large scale topography images (left column Figure 7). On these images, no bias voltage is applied because the metal–metal contact (tip–drain electrode) would cause instabilities. The current values are extracted from the current maps.

We note that as expected for p-type semiconductors $R_{NF}(l)$ and $R_{bp}$ are reduced at negative $V_G$. Table 1 confirms the observation made in Figure 6 and allows us to write the following equation

$$R_{bp} < 0.1\ R_{NF} \quad (3)$$

It means that the electrical resistance associated with the bridging of two (or more) individual NFs can be neglected with respect to the intrinsic resistance of the NFs. As complementary proof, we have measured the mobility of a web of P3BT NFs using the standard macroscopic OFET devices (channel length: 40 µm and channel width: 10 mm) in such a way that the extracted mobility is influenced by the transport within individual NFs but also by the bridging of NFs. We have measured a web mobility of $\mu_{WEB} = 0.05 \pm 0.01$ cm$^2$ V$^{-1}$ s$^{-1}$, remarkably close to the literature values $0.04 \pm 0.02$ cm$^2$ V$^{-1}$ s$^{-1}$[6,10,11] and, more importantly, comparable to our measurement on one single NF $\mu_{NF} = 0.07 \pm 0.03$ cm$^2$ V$^{-1}$ s$^{-1}$. This is a second proof that transport at the intersection of several NFs does not reduce or limit the charge transport process in a NFs network.

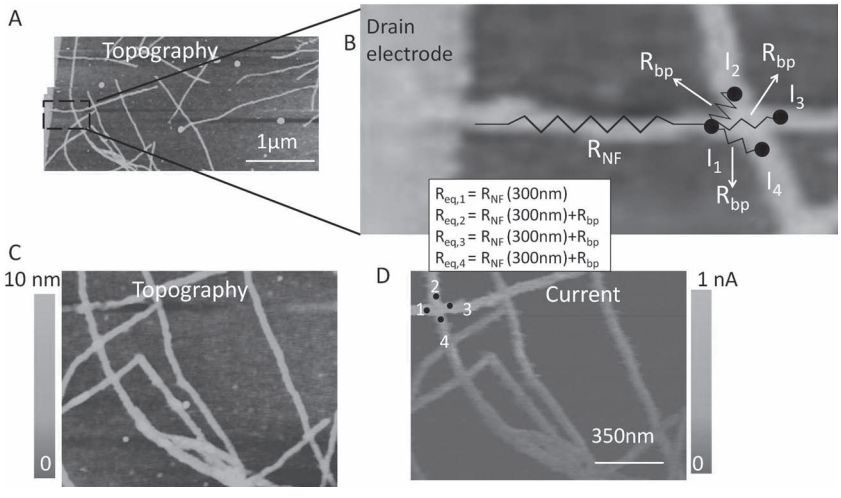


**Figure 6.** Electrical resistance evaluation of the bridging point of two NFs. A) Topography image of some NFs touching the drain electrode. B) Zoomed-in image of (A), the equivalent electrical circuit is shown. C,D) topography and current images of a part of (A) from which the four current values are extracted ($V_G = -4$ V and $V_D = 2$ V).

### 2.5. Structure of Bridging Points

Based on Equation (3) and on the thicknesses of bridging points of NFs, some information about how the NFs intersect can be deduced. Because of its higher resolution and softer contact than CAFM, tapping mode AFM has been extensively used to measure the thicknesses of NFs bridging points. Two kinds of intersections are observed: 1) the vast majority have four arms (noted here as X intersection) with a thickness between 6.5 and 8 nm and 2) the rest have three arms (noted here as T intersection) with a thickness of 4 nm. For the X intersection, since the intersection height is higher than 4 nm (height of one single NF) it means that the two NFs stack on each other

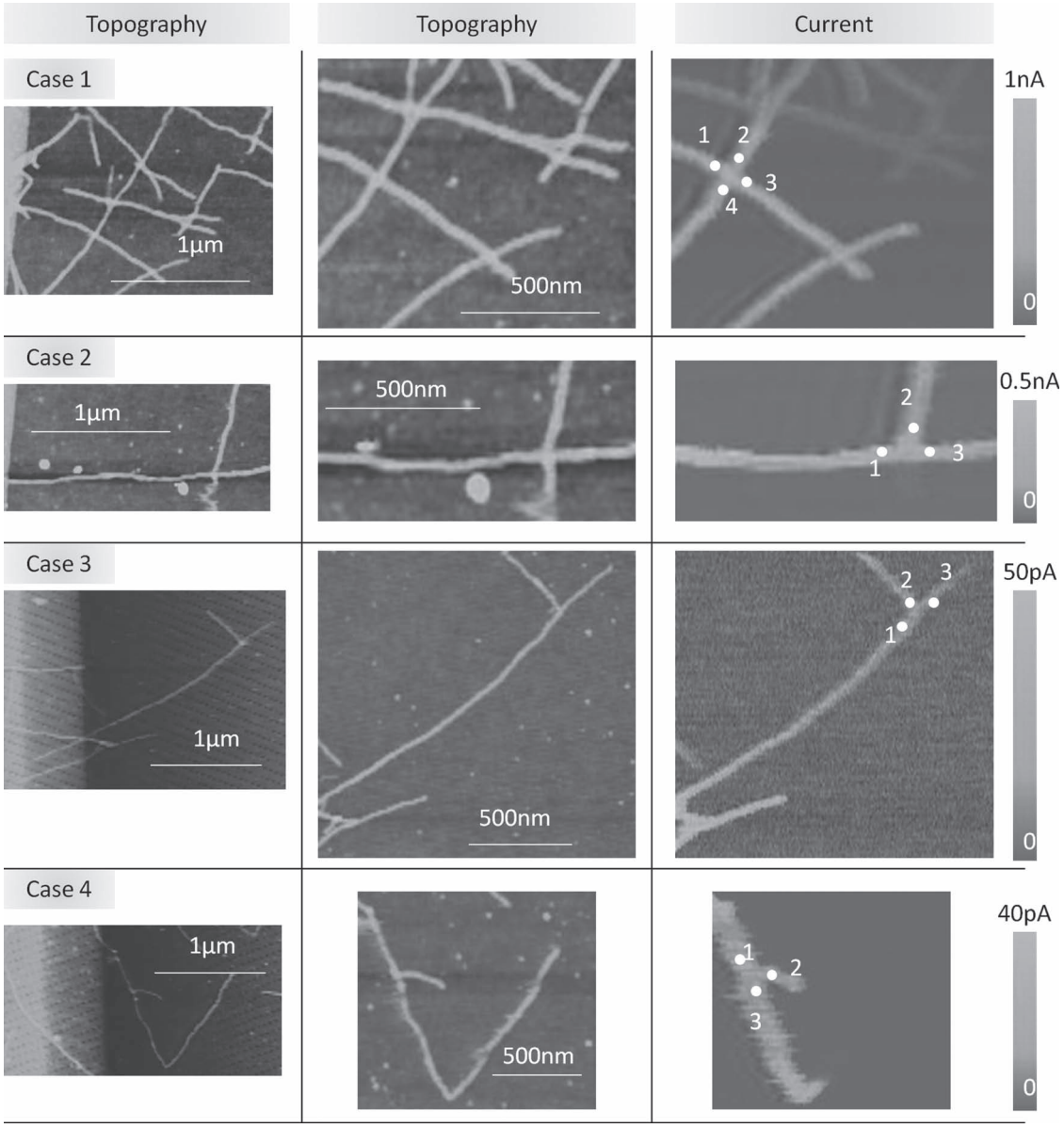


**Figure 7.** Four additional case studies to evaluate $R_{NF}(l)$ and $R_{bp}$. Left column is a large scale image including the drain electrode on the left extremity. Middle and right columns are a zoomed-in region of the left column. See Table 1 for numerical analysis.

and that the 8 nm X intersections correspond to a NFs superposition without interpenetration of the two NFs, as illustrated in **Figure 8**. In this configuration, their poor electrically conducting alkyl side chains touch each other leading to a high transport barrier for a hole going from NF1 to NF2 (or vice versa). This is in contradiction with Equation (3). Many papers in the literature have discussed the importance of tie molecules for conduction in conjugated polymers.[25]–[27] The tie molecules are molecular segments, which start in one crystalline domain and are connected to another crystalline domain. The edges of the P3BT NFs are expected to contain a lot of these loose polymer stands. The first reason is that the polydispersity of the NFs is not 1 but 2.1[8] and therefore there is a large variation in the length of the polymer chains, the longest ones being the tie molecules. The second argument for the presence of tie molecules comes from a paper of Zhang et. al.[28] They monitored the width of P3HT nanofibers as a function of the weight average molecular weight $M_w$. They found a linear trend for $M_w < 10$ kg mol$^{-1}$, which means that the width of one NF is proportional to the length of the polymer chain. On the other hand, for $M_w > 10$ kg mol$^{-1}$, they observed a constant width (at around 30 nm like our NFs) independent of $M_w$, which means that the polymer chains are folded inside the NFs or that some chains extend out of the NFs. The $M_w$ of our NFs is largely above the threshold value of 10 kg mol$^{-1}$ and this suggests that our NFs are composed of folded polymer chains and tie molecules. Thus, when the NFs are stacked on each other, the loose polymer strands can connect two different polymer chains and create conduction pathways

**Table 1.** Bias conditions, expressions for equivalent electrical resistance, measured currents and calculated $R_{NF}$, $R_{bp}$ values for the configurations of Figure 7. Case of Figure 6 is rewritten for convenience.

| Case | Bias | $R_{eq}$ | $I$ | $V_D = R_{eq,1}I_1 = R_{eq,2}I_2 = R_{eq,3}I_3 = R_{eq,4}I_4$ |
|---|---|---|---|---|
| 1 | $V_D$ = 2 V | $R_{eq,1} = R_{NF}$(600 nm) | $I_1$ = 380 pA | $R_{NF}$(600 nm) = 5.3 GΩ |
| | $V_G$ = –4 V | $R_{eq,2} = R_{NF}$(600 nm) + $R_{bp}$ | $I_2$ = 350 pA | $R_{bp}$ = 0.4 GΩ |
| | | $R_{eq,3} = R_{NF}$(600 nm) + $R_{bp}$ | $I_3$ = 350 pA | |
| | | $R_{eq,4} = R_{NF}$(600 nm) + $R_{bp}$ | $I_4$ = 380 pA | |
| 2 | $V_D$ = 2 V | $R_{eq,1} = R_{NF}$(1.5 μm) | $I_1$ = 221 pA | $R_{NF}$(1.5 μm) = 9.0 GΩ |
| | $V_G$ = –6 V | $R_{eq,2} = R_{NF}$(1.5 μm) + $R_{bp}$ | $I_2$ = 205 pA | $R_{bp}$ = 0.7 GΩ |
| | | $R_{eq,3} = R_{NF}$(1.5 μm) + $R_{bp}$ | $I_3$ = 220 pA | |
| 3 | $V_D$ = 2 V | $R_{eq,1} = R_{NF}$(1.6 μm) | $I_1$ = 18 pA | $R_{NF}$(1.6 μm) = 111.1 GΩ |
| | $V_G$ = –1 V | $R_{eq,2} = R_{NF}$(1.6 μm) + $R_{bp}$ | $I_2$ = 17 pA | $R_{bp}$ = 6.5 GΩ |
| | | $R_{eq,3} = R_{NF}$(1.6 μm) + $R_{bp}$ | $I_3$ = 18 pA | |
| 4 | $V_D$ = 4 V | $R_{eq,1} = R_{NF}$(500 nm) | $I_1$ = 13 pA | $R_{NF}$(500 nm) = 307.6 GΩ |
| | $V_G$ = 0 V | $R_{eq,2} = R_{NF}$(500 nm) + $R_{bp}$ | $I_2$ = 12 pA | $R_{bp}$ = 25.6 GΩ |
| | | $R_{eq,3} = R_{NF}$(500 nm) + $R_{bp}$ | $I_3$ = 12 pA | |
| Figure 6 | $V_D$ = 2 V | $R_{eq,1} = R_{NF}$(300 nm) | $I_1$ = 430 pA | $R_{NF}$(300 nm) = 4.6 GΩ |
| | $V_G$ = –4 V | $R_{eq,2} = R_{NF}$(300 nm) + $R_{bp}$ | $I_2$ = 420 pA | $R_{bp}$ = 0.4 GΩ |
| | | $R_{eq,3} = R_{NF}$(300 nm) + $R_{bp}$ | $I_3$ = 430 pA | |
| | | $R_{eq,4} = R_{NF}$(300 nm) + $R_{bp}$ | $I_4$ = 395 pA | |

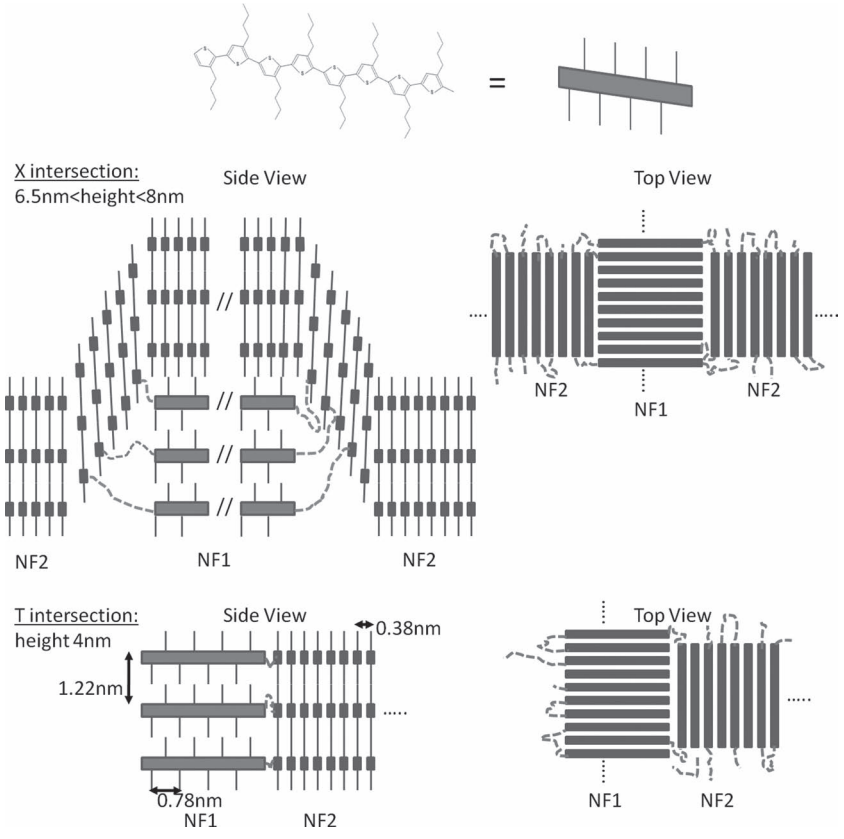


**Figure 8.** Schematics showing the structure of NFs bridging points for a X intersection (intersection with four arms) and a T intersection (intersection with three arms). Dashed line refers to tie molecules.

(Figure 8). In this way, the charge transport between both NFs is fast and Equation (3) is verified. For the 6.5 nm X intersections, there is presumably an interpenetrating distance of about 1.5 nm, which means that the highest polymer chain of the bottom NF is facing the lowest polymer chain of the top NF and holes can easily hop from one NF to the other without having to travel the alkyl side chains, thus the transfer is fast.

For the T-intersections, the situation is much different. Here, the two NFs are at the same level and, as shown on Figure 8, all the polymer backbones are facing each other leading to a fast hole transport between the NFs. However, we still expect tie molecules to be present and to reinforce the conduction mechanism.

## 3. Conclusion

In order to assess the nanoscale electrical properties of P3BT NFs, we have developed a transistor where one of the electrodes is the mobile CAFM tip. The contact resistance is estimated to be ≈4 kΩ cm, which does not limit the charge transport process and allows us to measure the mobility in one single NF: $\mu_{NF}$ = 0.07 ± 0.03 cm$^2$ V$^{-1}$ s$^{-1}$. A maximum current density of 20 kA cm$^{-2}$ in one single NF is measured without fiber destruction. By observing and analyzing the current images

in detail, we have found out that the bridging of two or more NFs does not reduce the charge transport process in a web of P3BT NFs ($R_{bp} < 0.1R_{NF}$). Therefore the hole mobility of one NF $\mu_{NF}$ is very similar to the mobility for a web of NFs $\mu_{WEB}$. For the 8 nm thick X intersections, this is explained by the presence of tie molecules. We consider that this technique can be extended to every electrically active nanostructure for which electrical characterization is needed.

## 4. Experimental Section

All the measurements were done on P3BT NFs as synthesized in ref. [8]. They result from the self-assembly of regioregular-P3BT chains. The number-average molecular weights ($M_n$) value [in kg mol$^{-1}$] as obtained by gel permeation chromatography versus polystyrene standards in chlorobenzene at 60 °C is (PDI in parentheses) 19.5 (2.29). Regioregularity as obtained by $^1$H-NMR is 96.5. Nanofiber dispersions were prepared by slow cooling of hot, filtered (0.45 µm) solution of well-dissolved polymer to room temperature in *o*-chlorotoluene and conditions that have been chosen to give over 75% fiber content while minimizing the formation of non-fibrillar aggregates.[8] An equilibrium state was obtained after 2 to ≈15 days after which the proportion of fibers to well-dissolved polymer remained constant over time.[8] Typical fiber heights and widths are 4 nm and 20 nm, respectively. When deposited on a transistor structure with appropriate high work function electrodes (such as Au or Pt), they behave like p-type semiconductors.[29] A Veeco multimode atomic force microscope equipped with the Nanoscope IIIa controller, the quadrex module, and the CAFM module was used. Two kinds of CAFM tips, giving similar results, were used: $PtIr_5$ coated tips from Nanosensors (Ref. PPP-CONTPt) and Au coated tips from Nanosensors (Ref. PPP-CONTAu), both with a spring constant of 0.2 N m$^{-1}$. Signal to noise ratio was optimized with a scan rate around 0.25 Hz. CAFM was carried out in contact mode with a low contact force (≈0.3 nN, deduced from force-curve measurements) to avoid any degradation of the soft polymer NFs. Assuming Young's modulus of ≈1 GPa for P3BT,[30] a tip radius of 25 nm (typical for CAFM tip), and using the Hertz mechanic model,[31] a contact radius of ≈2 nm was found. When taking current measurements, two verifications were routinely done. Suppose that one measured a stable positive current map for a positive $V_D$ and negative $V_G$. Firstly, it was verified that the current became zero when turning $V_D$ to zero and keeping $V_G$ negative. If not, this meant that the measured current was a leakage current reaching the gate electrode and the sample was disregarded. Secondly, it was verified that the current increased (decreased) when decreasing (increasing) $V_G$ and keeping $V_D$ constant. If not, this meant that the gate electrode was not well contacted. All the measurements were performed in a home-made glove box with an oxygen concentration lower than 50 ppm and humidity concentration lower than 10 ppm to avoid sample contamination and tip oxidation.

## Acknowledgements

This work was supported by the FWO (Fund for Scientific Research, Flanders, Belgium) project nanofibers R-1226, the IWT-SBO project Polyspec and the Interreg-project "Organext".

Received: September 3, 2011
Revised: November 14, 2011
Published online: January 17, 2012

[1] S. Bertho, W. D. Oosterbaan, V. Vrindts, J. D'Haen, T. J. Cleij, L. Lutsen, J. Manca, D. Vanderzande, *Org. Electron.* **2009**, *10*, 1248.
[2] B. Berson, R. De Bettignies, S. Bailly, S. Guillerez, *Adv. Funct. Mater.* **2007**, *17*, 1377.
[3] G. A. O'Brien, A. J. Quinn, D. A. Tanner, G. Redmond, *Adv. Mater.* **2006**, *18*, 2379.
[4] M. Arif, J. Liu, L. Zhai, S. I. Khondaker, *Appl. Phys. Lett.* **2010**, *96*, 243304.
[5] K. J. Ihn, J. Moulton, P. Smith, *J. Polym. Sci., Part B: Polym. Phys.* **1993**, *31*, 735.
[6] J. A. Merlo, C. D. Frisbie, *J. Polym. Sci., Part B: Polym. Phys.* **2003**, *41*, 2674.
[7] S. Samitsu, T. Shimomura, S. Heike, T. Hashizume, K. Ito, *Macromolecules* **2008**, *41*, 8000.
[8] W. D. Oosterbaan, V. Vrindts, S. Berson, S. Guillerez, O. Douhéret, B. Ruttens, J. D'Haen, P. Adriaensens, J. Manca, L. Lutsen, D. Vanderzande, *J. Mater. Chem.* **2009**, *19*, 5424.
[9] J. A. Merlo, C. D. Frisbie, *J. Phys. Chem. B* **2004**, *108*, 19169.
[10] S. Samitsu, T. Shimomura, S. Heike, T. Hashizume, K. Ito, *Macromolecules* **2010**, *43*, 7891.
[11] T. Shimomura, T. Takahashi, Y. Ichimura, S. Nakagawa, K. Noguchi, S. Heike, T. Hashizume, *Phys. Rev. B* **2011**, *83*, 115314.
[12] L. H. Jimison, M. F. Toney, I. McCulloch, M. Heeney, A. Salleo, *Adv. Mater.* **2009**, *21*, 1568.
[13] A. Salleo, *Mater. Today* **2007**, *10*, 38.
[14] L. S. C. Pingree, O. G. Reid, D. S. Ginger, *Adv. Mater.* **2009**, *21*, 19.
[15] J. M. Mativetsky, M. Palma, P. Samori, *Topics in Current Chemistry*, Exploring Electronic Transport in Molecular Junctions by Conducting Atomic Force Microscopy, **2008**, *285*, 157.
[16] J.-C. Bolsée, J. V. Manca, *Synth. Met.* **2011**, *161*, 789.
[17] C. Tanase, E. J. Meijer, P. W. M. Blom, D. M. de Leeuw, *Org. Electron.* **2003**, *4*, 33.
[18] A. Salleo, T. W. Chen, A. R. Völkel, Y. Wu, P. Liu, B. S. Ong, R. A. Street, *Phys. Rev. B* **2004**, *70*, 115311.
[19] Using the Hertz model, tip broadening can be written as $x = 2\sqrt{h(2R-h)}$. with $h$ = 4 nm (height of one NF) and $R$ = 25 nm (tip radius), we find $x$ =25 nm. Since true NF width is ≈20 nm (obtained from tapping mode AFM), we obtain a geometric width of 45 nm with CAFM.
[20] T. W. Kellie, C. D. Frisbie, *J. Vac. Sci. Technol. B* **2000**, *18*, 632.
[21] L. Burgi, T. J. Richards, R. H. Friend, H. Sirringhaus, *J. Appl. Phys.* **2003**, *94*, 6129.
[22] For a standard p-type transistor, the source and drain voltages are zero and negative. For our measurement, the source and drain voltages are zero and positive (2 V in Figure 5). In order to compare properly the data, we have to shift all our voltage by subtracting 2 V: our source and drain voltage are then negative (–2 V) and zero. Consequently, the transfer characteristic of Figure 5 has to be shifted to the left (negative values) by 2 V and thus $V_T = -4\ V \pm 1\ V$.
[23] G. A. O'Brien, A. J. Quinn, D. Iacopino, N. Pauget, G. Redmond, *J. Mater. Chem.* **2006**, *16*, 3237.
[24] C. Tanase, E. J. Meijer, P. W. M. Blom, D. M. de Leeuw, *Phys. Rev. Lett.* **2003**, *91*, 216601.
[25] M. Brinkmann, J. C. Wittmann, *Adv. Mater.* **2006**, *18*, 860.
[26] M. Brinkmann, P. Rannou, *Macromolecules* **2009**, *42*, 1125.
[27] M. J. Lee, D. Gupta, N. Zhao, M. Heeney, I. McCulloch, H. Sirringhaus, *Adv. Funct. Mater.* **2011**, *21*, 932.
[28] R. Zhang, B. Li, M. C. Lovu, M. Jeffries-EL, G. Sauvé, J. Cooper, S. Jia, S. Tristram-Nagle, D. M. Smilgies, D. N. Lambeth, R. D. McCullough, T. Kowalewski, *J. Am. Chem. Soc.* **2006**, *128*, 3480.
[29] W. D. Oosterbaan, J.-C. Bolsée, A. Gadisa, V. Vrindts, S. Bertho, J. D'Haen, T. J. Cleij, L. Lutsen, C. R. McNeill, L. Thomsen, J. V. Manca, D. Vanderzande, *Adv. Funct. Mater.* **2010**, *20*, 792.
[30] S. Miyauchi, T. Kondo, K. Oshima, T. Yamauchi, M. Shimomura, H. Mitomo, *J. Appl. Polym. Sci.* **2002**, *85*, 1429.
[31] According to the Hertz model, the contact radius $r$ is given by $r^3 = \frac{3FR}{4E}$ with $1/E = \frac{1-\nu_1^2}{E_1} + \frac{1-\nu_2^2}{E_2}$ where $F$ is the load, $R$ is the tip radius and $E$ is the Young's modulus. With $E_1$ = 195 GPa, $\nu_1$ = 0.38 for $PtIr_5$ and $E_2$ = 1 GPa, $\nu_2$= 0.35 for the polymer, $r$ is found to be around 2 nm.